Methodology for Earthquake Rupture Rate estimates of fault networks: example for the Western Corinth Rift, Greece

Thomas Chartier[1,2], Oona Scotti[2], Hélène Lyon-Caen[1] , Aurélien Boiselet[1,2*]

[1] Laboratoire de géologie, Ecole Normale Supérieure, CNRS UMR 8538, PSL Research University, Paris, 75005, France
[2] Bureau d'Evaluation des Risques Sismiques pour la Sûreté des Installations, Institut de Radioprotection et de Sûreté Nucléaire, Fontenay-aux-Roses, France
* now at Axa Global P&C, Paris, 75008, France.
Correspondence to: Thomas Chartier (chartier@geologie.ens.fr)

10

Abstract. Modelling the seismic potential of active faults is a fundamental step of probabilistic seismic hazard assessment (PSHA). An accurate estimation of the rate of earthquakes on the faults is necessary in order to obtain the probability of exceedance of a given ground motion. Most PSHA studies consider faults as independent structures and neglect the possibility of multiple faults or fault segments rupturing simultaneously (Fault to Fault -FtF- ruptures). The latest Californian model (UCERF-3) takes into account this possibility by considering a system level approach rather than an individual fault level approach using the geological , seismological and geodetical information to invert the earthquake rates. In many places of the world seismological and geodetical information along fault networks are often not well constrained. There is therefore a need to propose a methodology relying ~~only~~ on geological information alone to compute earthquake rate of the faults in the network. In the proposed~~is~~ methodology~~, similarly to UCERF-3~~, a simple distance criteria is used to define FtF ruptures and consider single faults or FtF ruptures as an aleatory uncertainty, similarly to UCERF-3. Rates of earthquakes on faults are then computed following two constraints: the magnitude frequency distribution (MFD) of earthquakes in the fault system as a whole must follow an ~~imposed~~ shape and the rate of earthquakes on each fault is determined by the specific slip-rate of each segment depending on the possible FtF ruptures. The modelled earthquake rates are then confronted to the available independent data (geodetical, seismological and paleoseismological data) in order to weigh different hypothesis explored in a logic tree.
The methodology is tested on the Western Corinth Rift, Greece (WCR) where recent advancements have been made in the understanding of the geological slip rates of the complex network of normal faults which are accommodating the ~15 mm/yr North-South extension. Modelling results show that geological, seismological ~~extension rates~~ and paleoseismological rates of earthquakes cannot be reconciled with only single fault rupture scenarios and require hypothesising a large spectrum of possible FtF rupture sets. Furthermore, in order to fit the imposed regional Gutenberg-Richter MFD target, some of the slip along certain faults needs to be accommodated either with interseismic creep or as post-seismic processes. Furthermore, computed individual fault's MFDs differ depending on the position of each fault in the system and the possible FtF ruptures associated with the fault. Finally, a comparison of modelled earthquake rupture rates with those deduced from the regional and local earthquake catalogue statistics and local paleosismological data indicates a better fit with the FtF rupture set constructed with a distance criteria based on a 5 km rather than 3 km, suggesting~~-~~ a high connectivity of faults in the WCR fault system.

a-priori chosen

1 Introduction

Probabilistic seismic hazard assessment (PSHA) is a method classically used to assess seismic hazard for a single site or for a group of sites hence creating a seismic hazard map. The first step of PSHA following a Cornell-McGuire (Cornell 1968, McGuire 1976) approach is the characterization of the seismic sources. For regions where active faults have been identified and their slip-rates are known ~~within a margin of error~~, several methods have been proposed in order to calculate the rate of earthquakes occurring on these faults. The most commonly used methods consider faults as independent structures on which

1

the strong earthquakes are located (SHARE Woessner et al, 2015; Yazdani et al, 2016; TEM ~~2015~~ Wang et al, 2016 ...). In these PSHA studies, a background seismicity will generate earthquakes up to a threshold magnitude of 6.0 or 6.5, beyond which earthquakes are generated on the faults. The rate of earthquakes for these larger magnitudes is based on geological and paleoseismological records, and the maximum magnitudes depend on the physical dimensions of the fault under consideration.

5 In the resulting model, the rate of lower magnitudes is controlled by seismological information and the rate of stronger magnitudes by geological information. In cases where large historical earthquakes are associated to multiple fault segments, the individual fault segments described by the geologists in the field are regrouped in a larger fault source and a mean slip rate is attributed to the fault source. A specific magnitude-frequency distribution (MFD), often Gutenberg-Richter (GR) (Gutenberg & Richter, 1944) or Characteristic Earthquake (Wesnouski, 1986), describing the mean slip-rate based earthquake rate on the

10 fault is attributed to each fault source. This process requires simplifying fault complexity in terms of geometry and slip-rate and doesn't allow complex ruptures that propagate from one fault source to an adjacent one.

In the past decades, the quality of the observation has improved and our understanding of earthquakes has grown. We observe more and more complex earthquake ruptures propagating on several neighboring faults. There is thus a need for hazard model to accurately represent the faults and ruptures complexity observed in the field by geologists.

15 In order to allow fault-to-fault (FtF) ruptures, the ~~WGCEP 2003~~ for San Francisco Bay Region developed a methodology that explores possible FtF ruptures in a logic tree. Each branch of the logic tree represents a seismic hazard model and the rate of the corresponding FtF rupture scenario is obtained by weighting the branches. Gulerce & Ocak 2013 used this approach and set the weight of each branch (or rupture scenario) in order to make the mean seismicity rate modeled by the logic tree fit the recorded seismicity around the fault of interest. This method treats the uncertainty of FtF ruptures as an epistemic uncertainty

20 in the PSHA calculation. Toro et al. (1997) define epistemic uncertainty as "uncertainty that is due to incomplete knowledge and data about the physics of the earthquake process. In principle, epistemic uncertainty can be reduced by the collection of additional information." Aleatory uncertainty on the other hand, is an "uncertainty that is inherent to the unpredictable nature of future events" (Toro et al 1997); in this respect FtF rupture should be treated as an aleatory uncertainty since it is linked to the randomness of the seismic phenomenon.

25 The latest Californian model UCERF-3 was developed using a novel methodology that treats all possible combinations of FtF rupture scenarios within the same branch of the logic tree as an aleatory uncertainty (Field et al, 2014). In their terminology, faults are divided in smaller sections and all possible section-to-section ruptures are investigated. The possibility of ruptures happening is controlled by a set of geometric and physical rules and the rate of earthquakes is computed using a "grand inversion" of the seismological, geological, paleosismological and geodetic data available in California. The regional

GR   geodetic?

30 ~~Gutenberg-Richter~~ MFD of earthquakes of California and the ~~GPS~~ deformation are used as a target for the total earthquake rupture forecast in each deformation model. This grand inversion relies also on estimates of the creep rate on faults deduced from local deformation data when available.

For many fault networks, only sparse seismological and geodetic data are available and the geological record is often the most detailed source of information concerning the faults' activity. In such cases, it's necessary to develop a methodology that

35 allows building seismic hazard models relying only on geological data and yet allowing FtF ruptures as an aleatory uncertainty. The sparse geodetical, seismological and paleoseismological data can then be used as a means of comparison to help weighting the different input hypothesis.

In this study we propose such a methodology based on slip-rate budget, FtF ruptures hypothesis and assumptions on the shape of the MFD defined for the fault system as a whole. The methodology is developed so as to be flexible and applicable to

40 regions where data on faults, geodesy and seismicity may be sparse. The rate of earthquakes on faults computed using geological information (slip-rates) is then compared to other sources of information such as the regional and local earthquake catalogues and the paleoseismic data in order to weigh the different epistemic uncertainty explored in the logic tree. Moreover, it is also known that faults accommodate important amounts of slip in either post-seismic slip or in creep events (e.g. L'Aquila

2

These phenomena, called Non-Main-Shock slip (NMS) later on, are integrated in the slip-rates deduced from geological information and should not be converted into earthquake rate when computing seismic hazard. The methodology presented in this study allows part of the geological slip-rate to be considered as NSM slip-rate.

We use this methodology to generate fault-based hazard models for the Western Corinth Rift (WCR), Greece, which has been

5   studied for the past decade by the Corinth Rift Laboratory Working Group (CRL-WG) (Lyon-Caen et al, 2004; Bernard et al, 2006; Lambotte et al, 2014). A large number of active faults have been identified in this area and a consensus about their possible geometries and activity rates has been reached within the CRL-WG (Boiselet, 2014). We used this geologic information to test our modelling approach and explore different epistemic uncertainties in a logic tree. Finally, we confront the modelled earthquake rates of each fault with seismological and paleoseismological data in order to weigh the hypothesis

10   in the logic tree.

2 Novel methodology for taking faults into account in PSHA

In most regions of the world the amount of data available to model faults in a PSHA study is often sparse and uncertain. However, the need to consider such data in PSHA is increasing and the methods to properly incorporate the available geological information in the hazard models are still missing. In this ~~optic~~ *context*, we propose to build a methodology that allows considering all

15   the available information on faults, allows setting rules to define FtF ruptures and considers single faults or FtF ruptures as an aleatory uncertainty. Our incremental method generates rates of earthquakes on faults by spending the slip-rate budget of each fault and following two rules: the resulting regional MFD of earthquakes in the whole ~~model~~ fault system follows an imposed shape and the rate of earthquakes on each fault is determined by the slip-rate on the fault. The shape of the individual MFD of each fault is not imposed.

20   The method requires a set of rupture scenarios as a list of the possible FtF ruptures in the fault model. In this study only a simple distance rule is used to define FtF ruptures. In future developments, more physics based approaches could be explored.

The proposed method is presented here in a nutshell and illustrated in Figure 1.

(1)   ~~List of~~ input data: *are gathered, they include:*

25   ▪   a definition of the 3D geometry of the fault system

     ▪   an estimate of the geological slip rates of each fault

Basic working (2)   ~~List of~~ hypothesis: *are stated, namely:*

     ▪   *some* suitable scaling laws to estimate the maximum magnitude each fault can host.

     ▪   *the* Minimum magnitude of earthquakes possible on the faults (5.0 in this study).

30   ▪   *the* possible FtF rupture scenarios.~~For instance,~~*;* in the example presented in Figure 1, three faults (*fault 1, fault 2* and *fault 3*) can rupture individually (F1, F2, F3) or in FtF rupture*s* (F1+F2, F2+F3 or F1+F2+F3)

     ▪   *the* shape of the ~~target~~regional MFD ~~target~~for the whole fault system. In this study a GR MFD distribution is assumed.

(3)   Computational steps : *are performed: they consist in:*

     ▪   ~~pre-c~~Calculation of all possible magnitude bins each fault and FtF rupture scenario can accommodate according to

35   the scaling law (Figure 1b).

     ▪   ~~and~~The slip-rate of each fault is spent in incremental quantities of slip-rate (*dsr*) that ~~each fault can accommodate by can be spent either an~~ along individual fault~~s~~ or ~~a~~ FtF rupture scenario~~s~~. In the example, the *fault 1, fault 2* and *fault 3* have a slip-rate budget of 5 mm/yr, 3.2 mm/yr and 4 mm/yr, respectively. *(see Fig. 1d)*

~~(4)~~ Incremental steps :

40   ❖   First, the bin of magnitude (of width 0.1) where this *dsr* will be spent is picked according to the regional MFD target expressed in terms of moment rate instead of rate of earthquakes (Figure 1 b). In this way large magnitudes have a

3

greater chance to be picked.

❖ Then, in this bin of magnitude M_i, a seismotectonic source Si (an individual fault or an FtF scenario) that can host this magnitude is picked randomly. The increment of moment rate $d\dot{M}_0$ for this source is calculated following equation 1 and the increment of rate of earthquakes dr_e is calculated using equation 2.

$$dM_0 = \mu . A . dsr \qquad (1)$$

$$dr_e(M_i) = \frac{d\dot{M}_0}{M_0(M_i)} \qquad (2)$$

where $d\dot{M}_0$ is the incremental increase of moment rate for the source S_i, μ the shear modulus of the fault (set at 30 GPa), A the area of the source and, dsr the increment of slip-rate spent, $dr_e(M_i)$ is the incremental increase of the rate of magnitude M_i and $M_0(M_i)$ is the seismic moment of a moment magnitude M defined by Hanks and Kanamori (1979) is:

$$M = \frac{2}{3}\log(M_0) - 10.7 \qquad (3)$$

❖ At each iteration, the slip-rate budget of the faults participating to the scenario accommodating the earthquakes of the three highest magnitude bins (0.3 being the range of uncertainties in the scaling laws used to assess the maximum magnitude) is checked:

➢ If there is still slip-rate budget to be spent, the dr_e calculated is added to the rate of earthquakes of magnitude M_i for the source S_i.

➢ If one of the faults of the FtF rupture generating the largest earthquake has exhausted its slip-rate budget, the final rates of the highest magnitude earthquakes is reached. Then knowing the shape of the imposed target MFD, the target rate at the fault system level for all magnitudes bins is known. At this stage, an additional check is made :

• if adding the dr_e calculated for magnitude M_i on the source S_i leads to exceed the target MFD for this magnitude, then this dr_e is not added to the source S_i and the increment dsr of this computation step is considered as Non Main-Shock (NMS) slip.

• if adding the dr_e to the source S_i does not lead to exceed the target MFD, this dr_e is added to the source S_i.

❖ As the magnitude bins are picked according to a distribution based on the moment rate, the greater magnitudes have more chance to be picked. Hence, the faults able to accommodate those magnitudes will see their slip-rate budget exhausted first. Once the faults involved in the largest possible magnitudes in the model don't have any more slip-rate to spend, the rate of larger magnitude bins is set. The target MFD for the whole fault-system is then calculated based on the imposed regional b value and the average rate of the three highest magnitude bins (0.3 being the range of uncertainties in the scaling laws used to assess the maximum magnitude). As the remaining slip-rate budget is consumed, an additional check is performed at each iteration to ensure that the earthquake rate of M_i in the fault system is lower than that predicted by the target MFD. When this condition is not satisfied, the dr_e calculated is not added to the rate of earthquakes of magnitude M_i for the source S_i but considered as Non Main-Shock (NMS) slip (Figure 1). The increment of slip-rate tal value dsr is then removed from the slip-rate budget of the fault or the faults involved in source S_i.

❖ Once If the fault's slip-rate budget of each fault reaches zero is exhausted, the fault and the corresponding FtF rupture scenarios the fault is involved in are removed and will cannot be picked anymore in subsequent steps iterations of the computation.

❖ These steps are repeated until all the slip-rate budgets of all the faults in the system reach zero.

The output of this process is an earthquake rupture rate ~~of~~ for different magnitudes for each fault and FtF rupture scenario in the model, considered as aleatory uncertainty. We also record how the slip-rate budget of each fault is spent between the different FtF ruptures and how much NMS-slip was needed on each fault in order to fit the target MFD shape (here GR MFD) with a given set of FtF rupture scenarios (Figure 1 d).

5 A simplified example of application of this methodology based on only two faults is given as an annex to this paper. This example illustrates step-by-step the way in which the proposed methodology allows to transform slip-rate budgets of faults into earthquake rates.

(4) Post-processing then includes:

~~(5)~~ Exploring the epistemic uncertainties:

Many assumptions have to be made when setting up the methodology (scaling law, FtF rupture set, faults parameters …)
10 and the different possible hypothesis should be explored in a logic tree.

~~(6)~~ Reality check :

The last step of the methodology involves comparing the modeled earthquake rates with independent data such as the seismicity rates deduced from the catalogue and from paleoearthquake rates deduced from trench studies. Each branch of the logic tree is then weighted according to its performance with this independant data.

15 In this study, we applied the proposed methodology to ~~the western Corinth Rift fault system.~~

a real, well documented rifting zone in the Peloponnese, Greece.

3 Application to the western Corinth rift fault system

The East West striking Corinth Rift is the most seismically active structure in Europe with several earthquakes larger than 5.5 recorded in the historical times as well as in the instrumental period (e.g. Jackson et al, 1982; Papazachos and Papazachou, 2003; Makropoulos et al, 2012). The Corinth Rift Laboratory (CRL) was set up in 2001 in the western and most seismically
20 active part of the rift (Lyon-Caen et al, 2004) with the goals of understanding the rifting process and providing key elements for the seismic hazard assessment of the region.

The GPS shows a highly localized opening of the Corinth Rift at a rate of 10 mm/yr in the east and 15 mm/yr in the west (Avallone et al. 2004) over a distance of around 20 km inducing a high strain-rate. This deformation is accommodated by a complex network of both north and south-dipping normal faults. Geological studies of these faults have shown that the north
25 dipping faults located on the southern coast have a higher slip-rate than the south-dipping northern faults, giving the rift its asymmetrical structure. In the south, the Peloponnese is uplifted by the activity of these faults (Armijo et al., 1996, Ford et al., 2013) and in the north the coast line is subsiding.

~~The Western Corinth Rift (WCR) fault system has been described by A. Boiselet in his PhD (Boiselet 2014, B14), defining geometries and slip-rates for each fault. The geological extension rate expressed by the sum of the horizontal projection of the~~
30 ~~slip-rates of the faults is in the range of 3 to 6 mm per year, three times less than the geodetic extension rate. Therefore, the WCR is a good candidate for an application of our methodology that relies only on geologic information to account for the large earthquakes that have been observed in the region (Albini et al 2017).~~

~~Figure 2 presents a map of the active faults of the WCR and their geological slip-rates. Only earthquakes of the complete period are represented on the map (Figure 2). In order to represent the epistemic uncertainty affecting the earthquake rates, we~~
35 ~~explore two different hypothesis of time of completeness of the catalogue: the times of completeness calculated by the SHARE project and the times of completeness calculated by Boiselet 2014 for the Corinth region (Table 1). The seismicity catalogue presented on Figure 2 is the catalogue SHEEC (Giardini et al., 2013; Stucchi et al., 2012; Grünthal et al., 2013) developed in the framework of the SHARE project updated for 6 historical earthquakes (based on Albini et al 2017) and 3 instrumental earthquakes (based on Baker et al 1997 study and personal communication from the 3-HAZ Corinth project). The updates and~~
40 ~~their implication on the catalogue are summarized in Table 2.~~

~~The fault geometries are presented in Figure 2 and the main parameters of the faults used here to test the proposed methodology are exposed in Table 3.~~ The faults slip-rates Western Corinth Rift (WCR) ~~are~~ were inferred from the displacement of geologic markers in the field or from seismic profiles ~~geological information~~ on each individual fault with the exception of the two blind 1995 and Pyrgos faults for which the microseismicity recorded close to the fault was transformed into slip-rate on the fault plane ~~[see Boiselet 2014]~~. These latter slip-rates are therefore subject to a very large uncertainty. The geological extension rate expressed by the sum of the horizontal projection of the geological slip-rates of the faults is in the range of 3 to 6 mm per year, three times less than the geodetic extension rate. ~~Therefore, the~~ Given this disagreement, the WCR is a good candidate ~~for an application of~~ to test if the earthquake rates calculated using our methodology that relies only on geological information ~~to~~ can account for the occurrence of large earthquakes ~~s~~ that have been observed in the region (Albini et al 2017).

The WCR fault system has been described by ~~A.~~ Boiselet ~~in his PhD~~ (~~Boiselet~~ 2014), defining a model for the fault system, including geometries and slip-rates for each fault (Figure 2, Table 1) and a set of possible FtF ruptures (hereafter model B14). The B14 model proposes a set of FtF rupture scenarios (Table 2~~4~~) assuming that two neighboring faults can make up a FtF scenario only if they are less than 3 km apart. In this paper, w~~W~~e propose to explore a logic tree branch with higher fault *also alternative rupture sets (see Fig. 3) with* connectivity (B14_hc) where faults can break together if their fault traces are separated by 5km or less therefore allowing a wider spectrum of possible FtF rupture scenarios (additional scenarios in green in Table 2~~4~~). As a comparison with classical fault PSHA studies, we ~~also~~ explore a branch with only simple fault rupture called B14_s. In this branch no FtF rupture is allowed.

b-value
The target MFD shape is chosen to be a GR with ~~a slope~~ of 1.15 ± 0.05 which is a typical value for extensional systems (Schorlemmer et al, 2005).
other
In this study we explore ~~different~~ epistemic uncertainties having potentially an impact on the modelled earthquake rates (Figure
in addition to the *previously described,* *have been*
3): ~~different~~ FtF rupture sets ~~as well as~~ two scaling laws (Wells and Coppersmith 1994 WC94 and Leonard 2010 Le10), used
using rupture area for normal faults
to calculate the maximum magnitude ~~that can occur on a fault according the fault area~~, and two values of the shear modulus μ (30 GPa and 20 GPa). ~~For each scaling law, the equation for normal faults linking the rupture area to the magnitude is used.~~ For each branch, 50 random samples are drawn from triangular distributions in order to explore the uncertainty in the b value of the target MFD (1.15 ± 0.05), in the slip-rate of the faults and ~~in~~ the uncertainty within the scaling law.

4 Modeled earthquake rupture rates and comparison with independent data

A first reality check is then
Using our method, we model the rate of earthquakes for the ~~western part of the Corinth Rift~~ WCR. It is possible to compare the modeled seismicity rate with the recorded one. *, for example by using* ~~To do so we use~~ the earthquake catalogue presented in figure 2. ~~The seismological moment rate is calculated directly using the rates of earthquake of each magnitude in the catalog using the moment magnitude equation (Hanks and Kanamori, 1979).~~ The seismicity catalogue presented on Figure 2 is the SHEEC catalogue (Giardini et al., 2013; Stucchi et al., 2012; Grünthal et al., 2013) developed in the framework of the SHARE project updated for 6 historical earthquakes (Albini et al., 2017) and 3 instrumental earthquakes (based on Baker et al 1997 study and personal communication from the 3-HAZ Corinth project). The updates and their implication on the catalogue are summarized in Table 3. We propagate the uncertainties on the earthquake ~~magnitudes and on the time of completeness of the~~ catalog in the estimate of seismic moment rate and earthquake rate calculations by randomly sampling the magnitude of each earthquake
within their *by.* *e* *In Table 4 the completeness*
~~with the~~ uncertainties (Stucchi et al 2012, Albini et al, 2017) and using two hypothesis of completeness ~~(Table 4): the times~~ for Greece calculated by the SHARE project (Stucchi et al., 2012) and the times calculated by Boiselet 2014 using the Stepp 1972 approach at the scale of the Corinth Rift region.
are reported.

The seismic moment in models B14 and B14_hc are in good agreement with the seismic moment deduced from the catalogue whereas the B14_s predicts a higher seismic moment rate (Figure 4a). This comparisons brings a better confidence in the models where FtF ruptures are possible than in the B14_s model. In the single-rupture model (B14_s), 90% to nearly 100 % of the geological slip-rate is converted into seismic moment rate with only less than 10% interpreted as NMS slip-rate. On the

other hand, when FtF ruptures are possible (B14 and B14_hc), 25% of the geological slip-rate budget of the faults is interpreted as NMS slip (Figure 4b).

The earthquake rates predicted by the different models can be compared to the rate of earthquakes in the catalogue as well (Figure 4c). The B14_s model doesn't manage to reproduce the rate of earthquake deduced from the catalogue, as it predicts a higher rate of magnitude 5 earthquakes and no earthquakes of magnitude 6.3 and above. On the other sidehand, we observe a good agreement of the MFDs of models B14 and B14_hc with the catalogue. B14 reproduces well the cumulative earthquake rate for magnitude 5.6 to 6.1 whereas model B14_hc reproduces better the cumulative rate of earthquakes of magnitude 5.0 to 5.5.

Slip-rate budget repartition

The way the slip-rate budget is spent between FtF rupture and single fault rupture and the NMS slip ratio of the fault depends on the slip-rate of the fault and the FtF ruptures the fault is involved in. Slow slipping faults that are involved in large FtF rupture scenario (Neos-Erineos or West Helike) have the majority of their slip-rate budget consumed by these large FtF ruptures (Figure 5). On the contrary, the fast slipping faults that are involved in few FtF ruptures scenarios (1995, Pyrgos, North-Eratini) spend their budget on predominantly single fault ruptures producing a high number of small to medium magnitude earthquakes which lead to easily exceed the GR regional target and thus imply a higher proportion of NMS slip-rate on these faults.

Models B14 and B14_hc have a similar mean 25% ratio of NMS slip ratio (Figure 4) but this ratio is not distributed between the different faults in the same way in each model. An important NMS proportion on the blind faults (Pyrgos and 1995-fault) and the off-shore North-Eratini fault is found for both models. There are three main factors that can induce this result: either the FtF sets are not realistic, the slip-rates explored on those faults are not realistic and don't include enough complex ruptures with these faults, or there is a mechanism of NMS slip such as creep or slow slip events happening on theses faults.

Earthquake rupture rate on the Aigion Fault

We choose now to focus our interest on the Aigion fault. Since this fault is one of the most active faults of the Western Corinth RiftWCR and crossing crosses the city of Aigion, it represents a major source of seismic hazard and risk for the region.

The earthquake rate modelled on the Aigion fault depends of the FtF rupture set allowed in the model (Figure 6). The resulting MFD of the Aigion fault has the shape of a GR for model B14 and B14_s, with a steeper slope for the B14_s model. In the B14_hc, the MFD computed offor the Aigion fault is more similar to a Characteristic Earthquake of magnitude close to 6.0, which is closesimilar to the maximum magnitude of earthquakes rupturing only the Aigion fault. It is worth noting that the larger magnitude earthquakes in Figure 6b and c involve not only the Aigion fault but also the neighbouring faults participating in the FtF ruptures (Figure 5, Table 2).

Using the paleoseismological data presented by Pantosti et al 2004, it is possible to propose rates of large magnitude earthquakes on the Aigion fault (figure 6). This paleorate is subject to large uncertainties but can be used to validate or invalidate the different FtF rupture set hypothesis. In the B14_s model where faults only break on their own, the Aigion fault is not able to accommodate the paleo-earthquake magnitudes. In the B14 model, where fault rupture is only allowed between faults separated by 3 km or less, the modelled earthquake rates are lower than the rates inferred from the paleosismological study. In the B14_hc model, where FtF ruptures are allowed for faults separated by 5km or less, the modelled earthquake rates agrees well with the paleorate, within the margin of uncertainty.

According to the recent reappraisal of the historical seismicity (Albini et al., 2017), the Aigion fault is most likely the source of the 1817 M 6.5 [6.0-6.5] and the 1888 M 6.2 [5.7 – 6.2] earthquakes. This leads to estimates of annual rates of M>6 earthquakes on the Aigion fault of 0.005 to 0.007 (Figure 6) depending on the completeness period used (Table 41). The model B14_s doesn't manage to reproduce the great magnitudes earthquakes observed in the catalogue. The annual rates for

earthquakes M>6 of 0.0034 and 0.0051 predicted by models B14 and B14_hc respectively are statistically compatible with the rate inferred from the catalogue.

5 Discussion: Weighting the logic tree branches

The comparison with independent local data allows suggesting weights for the different FtF rupture set hypothesis (Figure 3) for hazard calculation.

The B14_s branch, where faults can only rupture independently does not fit the annual moment rate, the earthquakes rate in the catalogue of the region nor the paleoearthquake magnitude on Aigion fault (Figure 4 and 6). We conclude that this branch should not be used for a hazard calculation in the Western Corinth Rift.

Between the two branches where FtF ruptures are possible, B14_hc manages to match the earthquake rate of the catalogue for a range of magnitudes where statistics are stronger (14 earthquakes of magnitude 5.0 and above) compared to the B14 model (matching only 4 earthquakes of magnitude 6.0 and above in the catalogue) (Figure 4). B14_hc branch matches the Aigion fault earthquake rate inferred from the paleoseismology and the historical catalogue better the B14 model (Figure 6). The agreement with the earthquake rate in the regional catalogue and the better reproduction of the Aigion fault data of the B14_hc model leads us to propose a stronger weight for this model compared to the B14 model for the estimate of hazard for Aigion city.

Conclusion

The methodology presented in this study uses a system level approach rather than an individual fault level approach to estimate the rate of earthquakes on faults based on the geological data collected for each fault and allowing FtF rupture in the hazard model as an aleatory uncertainty. The application of the methodology to the ~~Western Corinth Rift~~WCR fault network shows that in order to ~~model~~ match a GR MFD for the whole fault system, part of the fault slip-rates have to be spent as Non-Main-Shock slip. The way the fault slip-rate is distributed and the shape of the individual fault MFD depends ~~of~~ on the location of the fault in the network and the fault's characteristics. The earthquake rates modelled using the geological data on the faults are compared with the local earthquake catalogue and paleoseismic data in order to weigh the different epistemic hypothesis. In the case of the WCR, and for future seismic hazard assessment for the city of Aigion, these reality checks suggest ~~to~~ attribut~~ing~~e a stronger weight to the branch ~~with the 5 km distance criteria~~ for allowing FtF rupture between faults with the 5 km distance criteria (B14_hc), a lower weight to that based on the 3 km criteria (B14) and a null weight to the model where only single fault rupture~~s~~s a~~re~~e allowed (B14_s).

Perspectives

The fault network used for the application concerns only the western part of the Corinth Rift fault network. Integrating the rest of the network in the model could modify the final outcome and should be explored in future developments.

More reality checks will be implemented in the future in order to weigh the different uncertainties of the logic tree based on the results of the ongoing studies of the microseismicity in the WCR (i.e. use the possible presence of repeater earthquakes on the Aigion fault to validate NMS slip ratio - Duverger et al., 2015).

The methodology presented in this article can be applied to other fault systems, in different tectonic environments. In order to implement this approach, the geometries and slip-rates of the faults have to be known within uncertainties, FtF rupture scenarios sets have to be defined and the shape of the regional MFD needs to be assumed or inferred from the regional catalog. suitable?

If for the WCR the GR distribution seems adapted, it has been shown that a Youngs and Coppersmith distribution (Youngs

and Coppersmith, 1985) can be more appropriate for other fault systems (Hecker et al., 2013). ~~In such a case, the~~ methodology ~~can be applied in~~ applied in the same way for any other target MFD.

e.g. by *The flexibility of our* *permits it*

The earthquake rupture rate calculated using this methodology is very sensitive to the choice of possible FtF rupture scenarios. The comparison with the earthquake catalogue and local data such as the paleosismological data can provide guidance to the strength of each hypothesis. Nevertheless, the choice based on distance between faults should be supported by more physical approaches in the future such as Coulomb stress modeling (Toda et al., 2005) and dynamic modelling of the rupture (Durand et al., 2017).

The methodology at this stage doesn't consider the background seismicity. The example of the dense WCR fault system allowed setting aside this issue in order to test our methodology and focus on the FtF ruptures. Future developments of the methodology need to allow part of the modelled seismicity rate to be in the background. If performing hazard calculation for a region wider than the fault system itself, it is necessary to combine the models built with this methodology with classical area sources.

~~The fault network used for the application concerns only the western part of the Corinth Rift fault network. Integrating the rest of the network in the model could modify the final outcome and should be explored in future developments.~~

~~More reality checks will be implemented in the future in order to weigh the different uncertainties of the logic tree based on the results of the ongoing studies of the microseismicity in the WCR (i.e. use the possible presence of repeater earthquakes on the Aigion fault to validate NMS slip ratio - Duverger et al., 2015).~~

References

Albini P., A. Rovida, O. Scotti, and H. Lyon−Caen: Large Eighteenth–Nineteenth Century Earthquakes in Western Gulf of Corinth with Reappraised Size and Location, Bulletin of the Seismological Society of America doi: 10.17850120160181, 2017. ~~Large 18th−19th centuries earthquakes in Western Gulf of Corinth with reappraised size and location, submitted to BSSA, 121–133.~~

Armijo, R., Meyer, B., King, G., Rigo, A., and Papanastassiou, D.: Quaternary evolution of the Corinth Rift and its implications for the Late Cenozoic evolution of the Aegean. Geophysical Journal International 126(1), 1996.

Avallone, A., Briole, P., Agatza-Balodimou, A., Billiris, H., Charade, O., Mitsakaki, C., Nercessian, A., Papazissi, K., Paradissis, D. & Veis, G.: Analysis of eleven years of deformation measured by GPS in the Corinth Rift Laboratory area. Comptes Rendus Geosciences 336(4-5), 301-311, 2004.

Baker, C., Hatzfeld, D., Lyon-Caen, H., Papadimitriou, E. and Rigo, A., 1997, Earthquake mechanisms of the Adriatic Sea and western Greece, Geophys. J. Int. 131, 559-594, 2017.

Bernard, P., Lyon-Caen, H., Briole, P., Deschamps, A., Boudin, F., Makropoulos, K., Papadimitriou, P., Lemeille, F., Patau, G., and Billiris, H.: Seismicity, deformation and seismic hazard in the western rift of Corinth: new insights from the Corinth Rift Laboratory (CRL). Tectonophysics 426(1-2), 7–30, 2006.

Boiselet A.: Cycle sismique et aléa sismique d'un réseau de failles actives : le cas du rift de Corinthe (Grèce), PhD Thesis, 2014. https://hal.archives-ouvertes.fr/tel-01456400

Cornell, C. A.: Engineering seismic risk analysis. Bulletin of the Seismological Society of America, 58(5), 1583-1606, 1968).

Durand, V., Hok, S., Boiselet, A., Bernard, P., and Scotti, O.: Dynamic rupture simulations on a fault network in the Corinth Rift. Geophys J Int 2017; 208 (3): 1611-1622. doi: 10.1093/gji/ggw466.

Duverger, C., Godano, M., Bernard, P., Lyon-Caen, H., and Lambotte, S.: The 2003–2004 seismic swarm in the western Corinth rift: Evidence for a multiscale pore pressure diffusion process along a permeable fault system, Geophys. Res. Lett., 42, doi: 10.1002/2015GL065298, 2015.

Field, E. H., Arrowsmith, R. J., Biasi, G. P., Bird, P., Dawson, T. E., Felzer, K. R., Jackson, D. D., Johnson, K. M., Jordan, T. H., Madden, C., Michael, A. J., Milner, K. R., Page, M. T., Parsons, T., Powers P. M., Shaw, B. E., Thatcher, W. R., Weldon R. J., and Zeng Y.: Uniform California Earthquake Rupture Forecast, version 3 (UCERF3) The time-independent model. Bulletin of the Seismological Society of America, 104(3), 1122-1180, doi: 10.1785/0120130164, 2014.

Ford, M., Rohais, S., Williams, E. A., Bourlange, S., Jousselin, D., Backert, N., and Malatre, F.: Tectono-sedimentary evolution of the Western Corinth Rift (Central Greece), Bassin Research, doi: 10.1111/j.1365-2117.2012.00550.x, 2013.

Giardini, D., J. Woessner, L. Danciu, H. Crowley, F. Cotton, G. Grünthal, R. Pinho, G. Valensise, S. Akkar, R. Arvidsson, R. Basili, T. Cameelbeeck, A. Campos-Costa, J. Douglas, M. B. Demircioglu, M. Erdik, J. Fonseca, B. Glavatovic, C. Lindholm, K. Makropoulos, F. Meletti, R. Musson, K. Pitilakis, K. Sesetyan, D. Stromeyer, M. Stucchi, A. Rovida: Seismic Hazard Harmonization in Europe (SHARE): Online Data Resource, http://portal.share-eu.org:8080/jetspeed/portal/, doi: 10.12686/SED-00000001-SHARE, 2013.

Grünthal, G., Wahlström, R., and Stromeyer, D.: The SHARE European Earthquake Catalogue (SHEEC) for the time period 1900-2006 and its comparison to EMEC. Journal of Seismology, 17, 4, 1339-1344, doi: 10.1007/s10950-013-9379-y, 2013.

Gülerce, Z. and Ocak, S.: Probabilistic seismic hazard assessment of Eastern Marmara Region. Bulletin of Earthquake Engineering, 11(5), 1259-1277, 2013.

Gutenberg, B., and Richter, C.: Frequency of earthquakes in California, Bull. Seismol. Soc. Am. 34, 185–188, 1944.

Hanks, T. C., and Kanamori, H.: A moment magnitude scale, J. Geophys. Res., 84(B5), 2348–2350, doi: 10.1029/JB084iB05p02348, 1979.

Hanks, T. C., and Bakun W. H.: M- log A observations for recent large earthquakes, Bull. Seismol. Soc. Am. 98, 490–494, 2008.

Hecker, S., Abrahamson, N. A., and Wooddell, K. E.: Variability of Displacement at a Point: Implications for Earthquake-Size Distribution and Rupture Hazard on Faults, Bulletin of the Seismological Society of America vol. 103 no. 2A, 651-674, doi: 10.1785/0120120159, April 2013.

Jackson, J., Gagnepain, J., Houseman, G., King, G., Papadimitriou, P., Soufleris, C., and Virieux, J.:. Seismicity, normal faulting, and the geomorphological development of the Gulf of Corinth (Greece): the Corinth earthquakes of February and March 1981. Earth and Planetary Science Letters 57(2), 377–397, 1982.

Lambotte, S., Lyon-Caen, H., Bernard, P., Deschamps, A., Patau, G., Nercessian, A., F. Pacchiani, S. Bourouis, M. Drilleau, and Adamova, P.: Reassessment of the rifting process in the Western Corinth Rift from relocated seismicity. Geophys. J. Int. (2014) 197, 1822–1844 doi: 10.1093/gji/ggu096, 2014.

Leonard, M.: Earthquake fault scaling: Self-consistent relating of rupture length, width, average displacement, and moment release. Bulletin of the Seismological Society of America, 100(5A), 1971-1988. doi: 10.1785/0120090189, 2010.

Lyon-Caen, H., Papadimitriou, P., Deschamps, A., Bernard, P., Makropoulos, K., Pacchiani, F., and Patau, G.: First results of the CRLN seismic network in the western Corinth Rift: evidence for old-fault reactivation. Comptes Rendus Geoscience, 336(4), 343-351, 2004.

Makropoulos, K., Kaviris, G., and Kouskouna, V.: An updated and extended earthquake catalogue for Greece and adjacent areas since 1900. Natural Hazards and Earth System Sciences 12(5), 1425–1430, 2012.

McGuire, R. K.: FORTRAN computer program for seismic risk analysis (No. 76-67). US Geological Survey, 1976.

Papazachos, B.C., and Papazachou C.: The earthquakes of Greece. Ziti Publ. Co., Thessaloniki, Greece, pp 286 (in Greek), 2003.

Pantosti, D., De Martini, P. M., Koukouvelas, I., Stamatopoulos, L., Palyvos, N., Pucci, S., Lameille, F., and Pavlides, S.: Palaeoseismological investigations of the Aigion Fault (Gulf of Corinth, Greece). Comptes Rendus Geoscience, 336(4), 335-342, 2004.

Schorlemmer, D., Wiemer, S., and Wyss, M.: Variations in earthquake-size distribution across different stress regimes. Nature, 437(7058), 539-542, 2005.

Stepp, J.C.: Analysis of completeness of the earthquake sample in the Puget Sound area and its effect on statistical estimates of earthquake hazard. Proc. of the 1st Int. Conf. on Microzonazion, Seattle, vol. 2, pp. 897–910, 1972.

Stucchi, M., Rovida, A., Gomez Capera, A. A., Alexandre, P., Camelbeeck, T., Demircioglu, M. B., Gasperini, P., Kouskouna, V., Musson, R. M. W., Radulian, M., Sesetyan, K., Vilanova, S., Baumont, D., Bungum, H., Fäh, D., Lenhardt, W., Makropoulos, K., Martinez J. M., Solares, Scotti, O., Živčić, M., Albini, P., Batllo, J., Papaioannou, C., Tatevossian, R., Locati, M., Meletti, C., Viganò, D., and Giardini D.: The SHARE European Earthquake Catalogue (SHEEC) 1000–1899. Journal of Seismology, doi: 10.1007/s10950-012-9335-2, 2012.

Stucchi, M., Rovida, A., Capera, A. G., Alexandre, P., Camelbeeck, T., Demircioglu, M. B. and Sesetyan, K.: The SHARE European earthquake catalogue (SHEEC) 1000–1899. Journal of Seismology, 17(2), 523-544., 2013.

Toda, S., Stein, R. S., Richards-Dinger, K., and Bozkurt, S. B.: Forecasting the evolution of seismicity in southern California: Animations built on earthquake stress transfer, J. Geophys. Res., 110, B05S16, doi: 10.1029/2004JB003415, 2005.

Toro, G. R., Abrahamson, N. A., and Schneider, J. F.: Model of strong ground motions from earthquakes in central and eastern North America: best estimates and uncertainties. Seismological Research Letters, 68(1), 41-57, 1997.

Wang, Y.J., Lee, Y.T., Chan, C.H., Ma, K.F.: An Investigation of the Reliability of the Taiwan Earthquake Model PSHA2015, Seismological Research Letters Nov 2016, 87 (6) 1287-1298; doi: 10.1785/0220160085, 2016.

Wells, D. L., and Coppersmith, K. J.: New empirical relationships among magnitude, rupture length, rupture width, rupture area, and surface displacement. Bulletin of the seismological Society of America, 84(4), 974-1002, 1994.

Woessner, J., Laurentiu, D., Giardini, D., Crowley, H., Cotton, F., Grünthal, G., Valensise, V., Arvidsson, R., Basili, R., Betül Demircioglu, M., Hiemer, S., Meletti, C., Musson, R. W., Rovida, A. N., Sesetyan, K., and Stucchi, M.; The SHARE Consortium : The 2013 European Seismic Hazard Model: key components and results, Bull Earthquake Eng (2015) 13: 3553. doi:10.1007/s10518-015-9795-1, 2015.

Working Group on California Earthquake Probabilities: Earthquake Probabilities in the San Francisco Bay Region: 2002–2031, USGS Open-File Report 03-214, 2003.

Yazdani, A., Nicknam, A., Eftekhari, S. N., and Dadras, E. Y.: Sensitivity of Near-Fault PSHA Results to Input Variables Based on Information Theory. Bulletin of the Seismological Society of America, Vol. 106, No. 4, pp. 1858–1866, August 2016, doi: 10.1785/0120160006, 2016.

Youngs, R. R., and Coppersmith, K. J.: Implications of Fault Slip Rates and Earthquake Recurrence Models to Probabilistic Seismic Hazard Estimates, Bulletin of the Seismological Society of America, Vol. 75, No. 4, pp. 939-964, August 1985.
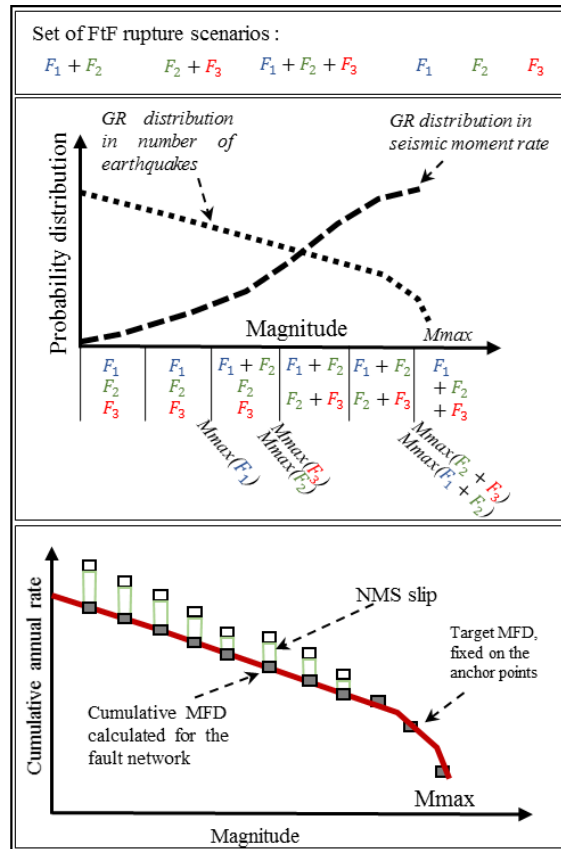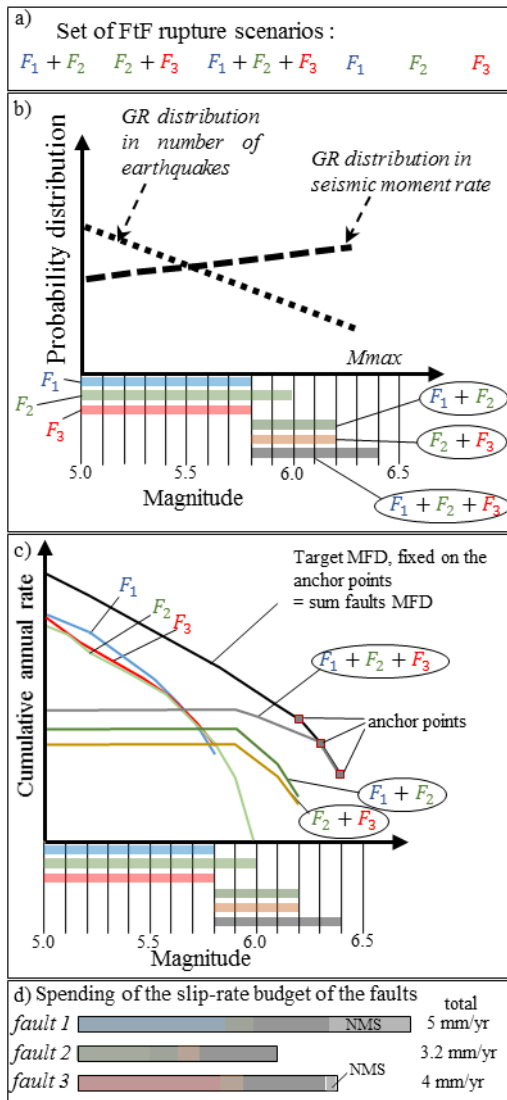
Figure 11 : Illustration of the methodology. ~~Top:a)~~ ~~set~~Set of FtF rupture scenarios. ~~Middle:b)~~ ~~picking~~Picking of the magnitude bins and of the sources. ~~Bottom:c)~~ ~~fit~~ Building~~to~~ the target MFD ~~: and calculation of the NMS slip proportion. Grey squares represent the cumulative annual rate of earthquakes modeled in the fault system; white squares represent the proportion of earthquake rates that the fault system would produce if no NMS was considered;~~ the ~~red~~ black curve is the target MFD anchored at the mean of the three highest magnitude bins (magnitude bin of 0.1). The sum of the MFD of the six sources is equal to the target MFD. d) visualization of the way each fault's slip-rate budget is spent (colors correspond to the individual rupture or the FtF rupture, NMS : Non Main Shock slip).
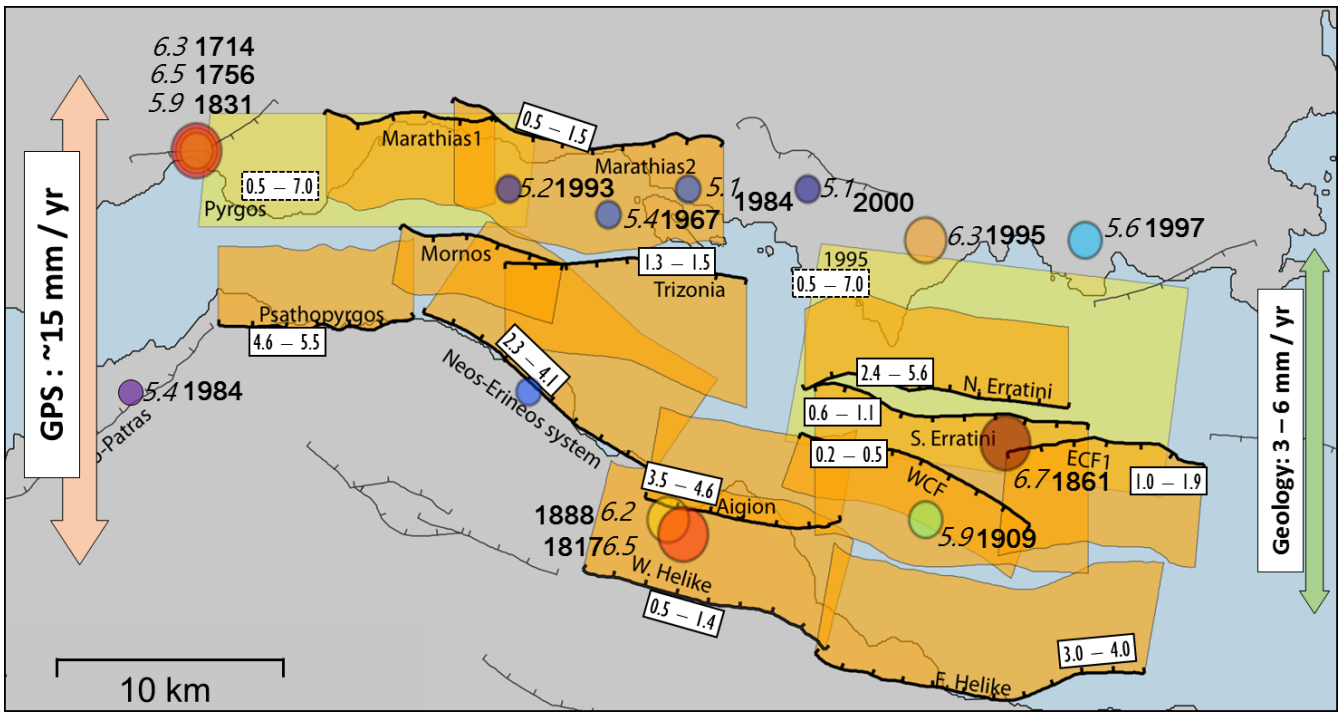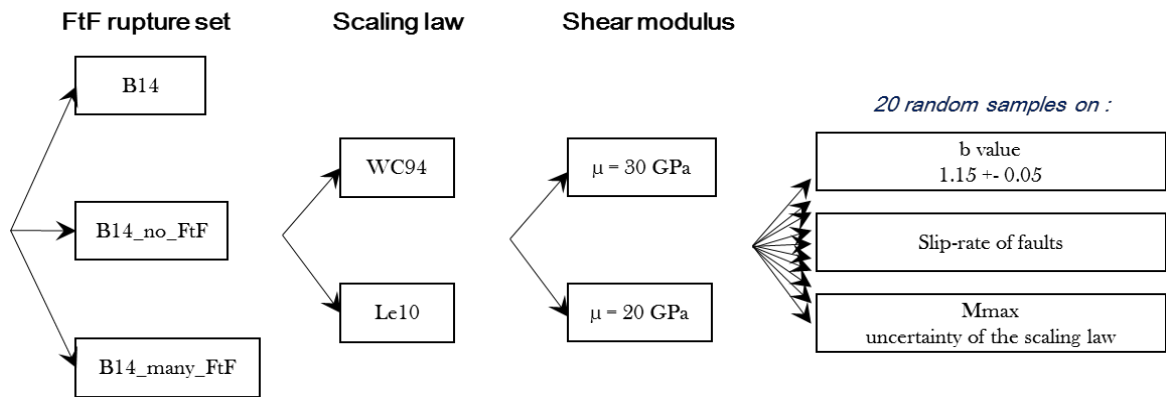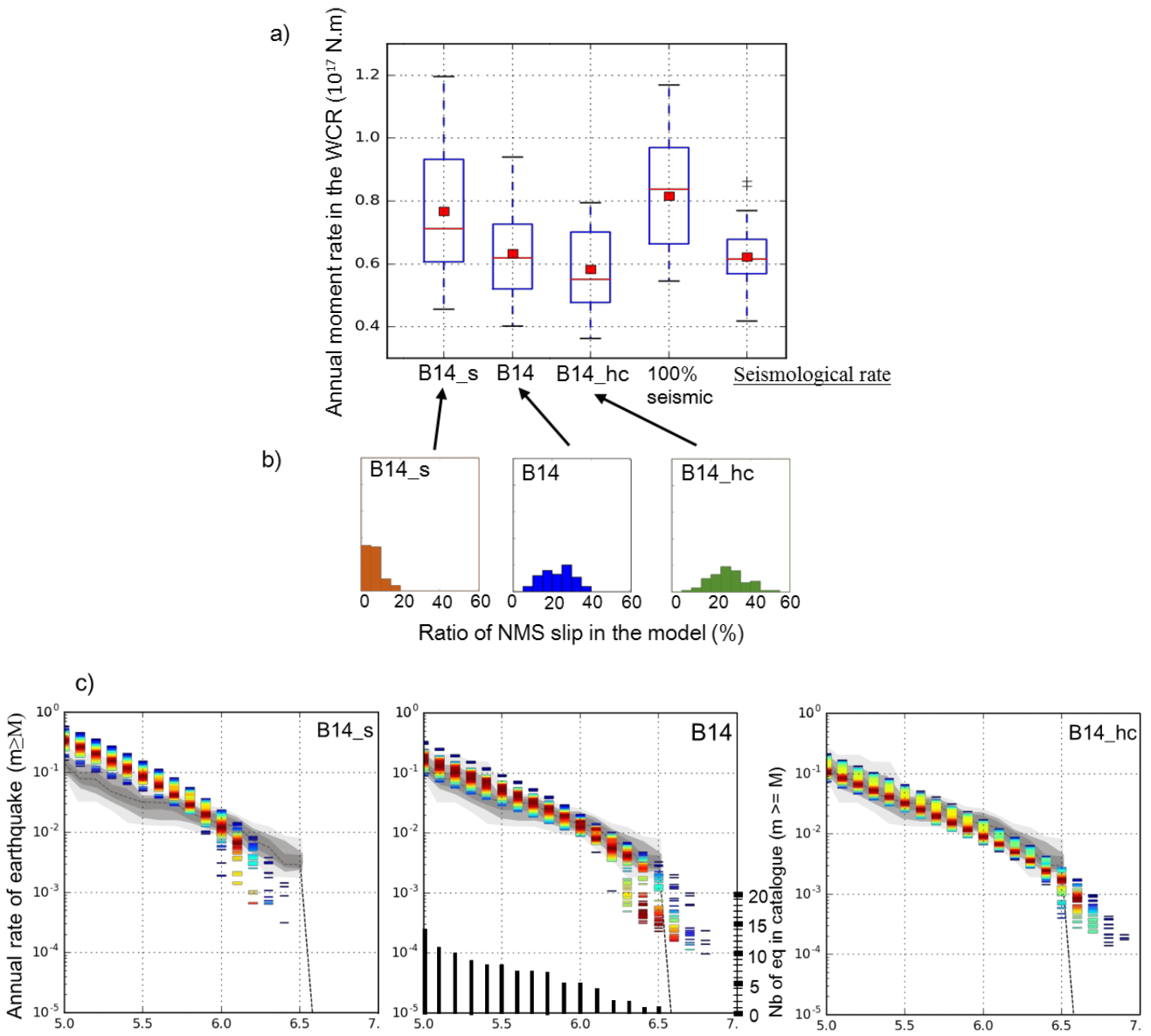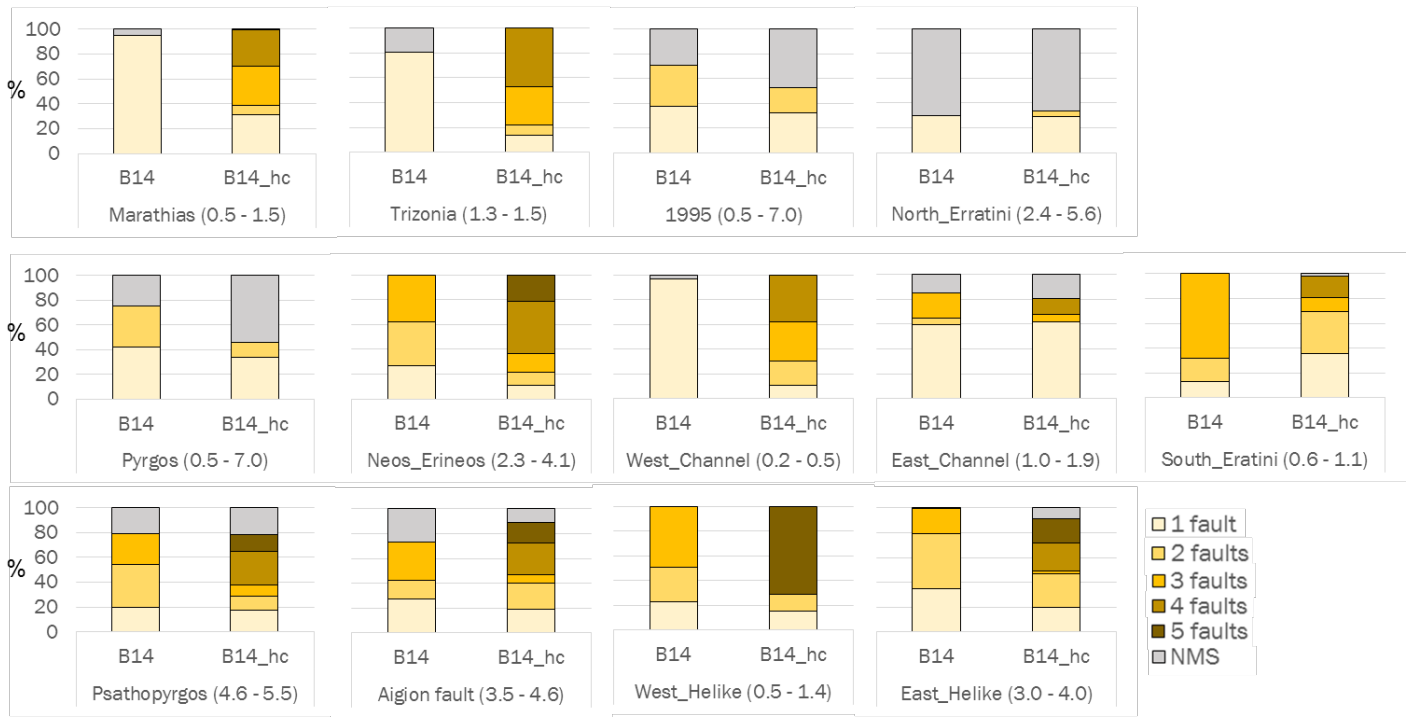
Figure 22 : Map of the active faults of the western part of the Corinth Rift (modified from Boiselet 2014). Earthquakes of the catalogue during the complete period represented by the circles with color and size depending on the magnitude. Year and preferred magnitude of earthquake indicated. The minimum and maximum values (mm/yr) of the slip-rates of the faults are indicated in the boxes. The green arrow shows an approximation of the rift extension calculated by projecting horizontally the faults slip-rate and the pink arrow shows the extensional rate of the rift measured by GPS. The orange polygons are the projections to the surface of the active faults. The yellow polygons are the projection to the surface of the blind faults (Pyrgos fault and 1995 fault).
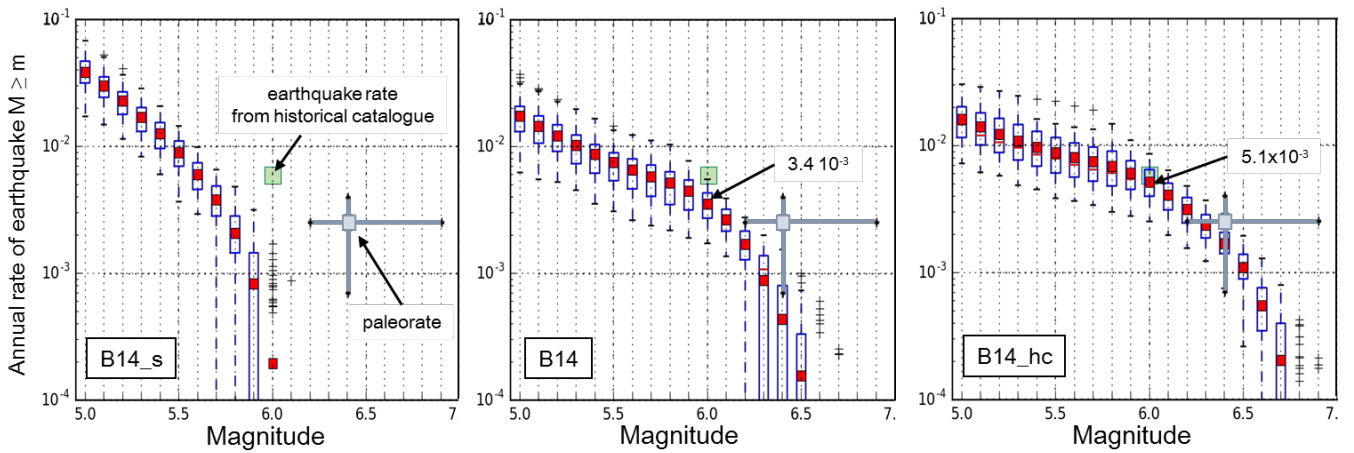

Figure 33 : Logic tree explored for this study

Figure 44 : Modelled seismicity for the WCR fault network and comparison to the seismicity rate based on the earthquake catalogue of the complete period. a): comparison between the modelled moment rates for each FtF scenario set and the seismological rate calculated from the earthquake catalogue. Each box represents the standard deviation around a mean and median value represented by a red square and a red line respectively. From left to right: the three first boxes are for each hypothesis of scenario set in the logic tree, the fourth box shows the moment rate assuming 100% of the slip-rate of faults is converted into seismic moment, the fifth box shows the moment rate calculated from the earthquake catalogue. **b):** distribution of the ratio of NMS slip resulting from the three deformation models. **c):** Comparison between the modelled GR MFD deduced from geological data for the whole fault system and that deduced from the WCR catalogue. The models are represented as a colored density function with the red colors for the rates predicted by the higher number of models. The cumulative rates calculated from the catalogue are shown as a grey density function. The cumulative number of earthquakes in the catalogue is indicated by black bars in the central figure.

14

Figure 55 : Visualization of the way the slip-rate budget of each fault is spent. The color depends on the number of faults involved in the FtF rupture. Minimum and maximum values of the slip-rate on each fault is shown in brackets in mm/yr.

5

Figure 66 : Rate of earthquakes occurring on the Aigion fault for each FtF rupture set. Variability resulting from the exploration of the logic tree is illustrated by the blue boxes. The annual rates of M≥6 earthquakes on Aigion fault is indicated for the B14 and B14_hc models. The grey square represents the paleorate interpreted from Pantosti et al. (2004) and its uncertainties. The green box represents the rate of earthquakes greater than magnitude 6 on the Aigion fault inferred from the historical catalogue.

10

fault name	Length	dip	seismogenic depth (km) upper	lower	slip-rate (mm/yr) min	Mean	max	Mmax (WC94)	time frame of the data
Psathopyrgos_fault	8.5	60	0	6	4.6	5	5.5	5.8	2 kyr
Neos_Erineos_fault	11.4	55	0	7	2.3	3.2	4.1	6.0	3 – 4 kyr
Aigion_fault	8.6	60	0	7	3.5	4	4.6	5.8	50-60 kyr
East_Helike_fault	14 .5	55	0	7	3	3.5	4	6.1	10-12 kyr
West_Helike_fault	11.2	55	0	7	0.5	0.9	1.4	6.0	800 kyr
Trizonia_fault	10.6	65	0	7	1.3	1.4	1.5	5.9	800 kyr
West_Channel_fault	10.8	45	0	2.5	0.4	0.45	0.5	5.6	240 - 400 kyr
South_Eratini_fault	12	45	0	6.5	0.6	1	1.4	6.0	800 kyr
East_Channel_fault	22	45	0	4.5	1	1.4	1.8	5.7	1500 kyr
North_Erratini_fault	11.5	60	0	6	2.4	4	5.6	5.9	12 kyr
Marathias_fault	17.4	60	0	6.5	1.39	1.4	1.41	6.1	400 kyr
1995_fault	14	35	8	12	0.5	3.2	7	6.0	5 yr
Pyrgos_fault	11	35	6	11	0.5	3.2	7	6.1	5 yr

Table 1: Fault characteristics in Boiselet, 2014. Mmax calculated using Wells and Coppersmith equation for normal faults.

FtF set	Faults involved in the scenario				Mmax
	All single fault rupture scenarios +				
	Aigion	Neos_Erineos			6.2
	Aigion	Neos_Erineos	Psathopyrgos		6.4
	Neos_Erineos	Psathopyrgos			6.2
	East_Helike	West_Helike			6.3
	Psathopyrgos	Pyrgos			6.2
B14	East_Helike	1995			6.4
	East_Helike	South_Eratini			6.4
	East_Helike	South_Eratini	West_Helike		6.5
	East_Helike	South_Eratini	East_Channel		6.5
	South_Eratini	East_Channel			6.2
	Marathias	Trizonia			6.3
	Marathias	Trizonia	Psathopyrgos		6.4
	Marathias	Trizonia	Neos_Erineos		6.5
	Marathias	Trizonia	Neos_Erineos	Psathopyrgos	6.6
	Aigion	West_Helike			6.2
	Aigion	West_Channel			5.8
	Aigion	East_Channel	West_Channel		6.2
	Aigion	South_Eratini	East_Channel	West_Channel	6.4
B14_hc	Aigion	East_Helike	Neos_Erineos	Psathopyrgos	6.5
	East_Helike	West_Channel			6.2
	East_Helike	South_Eratini	West_Channel		6.4
	East_Helike	South_Eratini	East_Channel	West_Channel	6.5
	South_Eratini	North_Eratini			6.3
	Aigion	Trizonia	Neos_Erineos	Psathopyrgos	6.5
	Aigion	1995			6.2
	Aigion	East_Helike			6.3
	South_Eratini	East_Channel	West_Channel		6.3

	Aigion	East_Helike	West_Helike	Neos_Erineos	Psathopyrgos	6.6

Table 2: FtF rupture scenarios considered in addition to the single fault rupture scenarios. The lines in black are included in all the branches of the logic tree. The lines in green are included only in the branch B14_hc. Branch B14_s only allows simple fault ruptures. Mmax are calculated using the Wells and Coppersmith relation for normal faults.

Date	Type of update	Old parameters	New parameters	Special implication for the catalogue
1748 May 14	Magnitude	M = 6.4 +- 0.25	M = 5.9 [5.4 – 5.9]	Not in the complete period for this range of magnitudes
1817 Aug 23	Magnitude	M = 6.6 +- 0.25	M = 6.5 [6.0 – 6.5]	
1861 Dec 26	Location	(38.22, 22.139)	(38.28, 22.24)	Not associated with Aigion fault
1888 Sep 9	Magnitude	M = 6.3 +- 0.4	M = 6.2 [5.7 – 6.2]	
1889 Aug 25	Location and Magnitude	(38.25, 22.08) M = 6.24 +- 0.25	(38.50, 21.33) M = 6.4 [6.4 – 6.6]	Earthquake outside the WCR
1965 Mar 3	Depth and Magnitude	Depth = 10 km M = 6.5	Depth = 55 km M = 6.8	Earthquake associated with the subduction zone, not with the WCR fault system
1995 Jun 15	Location and Magnitude	(38.37, 22.15) M = 5.8	(38.36, 22.20) M = 6.3	
1997 Nov 05	Location	(22.28,38.41)	(22.28,38.36)	

Table 3: Earthquakes updated in the historical and instrumental catalogues of the Western Corinth Rift

SHARE project		Boiselet 2014	
Magnitude range	Date of completeness	Magnitude range	Date of completeness
4.1 – 5.1	1970	5.0 – 5.4	1958
5.1 – 5.7	1900	5.5 – 6.0	1904
5.7 – 6.5	1650	6.0 – 6.5	1725
≥ 6.5	1450	6.5 – 7.0	1725

Table 1 4: Completeness hypothesis explored in this study.

~~Date~~	~~Type of update~~	~~Old parameters~~	~~New parameters~~	~~Special implication for the catalogue~~
~~1748 May 14~~	~~Magnitude~~	~~M = 6.4 +- 0.25~~	~~M = 5.9 [5.4 – 5.9]~~	~~Not in the complete period for this range of magnitudes~~
~~1817 Aug 23~~	~~Magnitude~~	~~M = 6.6 +- 0.25~~	~~M = 6.5 [6.0 – 6.5]~~	
~~1861 Dec 26~~	~~Location~~	~~(38.22, 22.139)~~	~~(38.28, 22.24)~~	~~Not associated with Aigion fault~~
~~1888 Sep 9~~	~~Magnitude~~	~~M = 6.3 +- 0.4~~	~~M = 6.2 [5.7 – 6.2]~~	
~~1889 Aug 25~~	~~Location and Magnitude~~	~~(38.25, 22.08) M = 6.24 +- 0.25~~	~~(38.50, 21.33) M = 6.4 [6.4 – 6.6]~~	~~Earthquake outside the WCR~~
~~1965 Mar 3~~	~~Depth and Magnitude~~	~~Depth = 10 km M = 6.5~~	~~Depth = 55 km M = 6.8~~	~~Earthquake on the subduction plane, not in the WCR~~

| 1995 Jun 15 | Location and Magnitude | (38.37, 22.15) M = 5.8 | (38.36, 22.20) M = 6.3 | |
| 1997 Nov 05 | Location | (22.28,38.41) | (22.28,38.36) | |

Table 2 : Earthquakes updated in the historical and instrumental catalogues of the Western Corinth Rift

fault name	Length	dip	seismogenic depth (km) upper	lower	slip-rate (mm/yr) min	Mean	max	Mmax (WC94)	time frame of the data
Psathopyrgos_fault	8.5	60	0	6	4.6	5	5.5	5.8	2 kyr
Neos_Erineos_fault	11.4	55	0	7	2.3	3.2	4.1	6.0	3 – 4 kyr
Aigion_fault	8.6	60	0	7	3.5	4	4.6	5.8	50-60 kyr
East_Helike_fault	14 .5	55	0	7	3	3.5	4	6.1	10-12 kyr
West_Helike_fault	11.2	55	0	7	0.5	0.9	1.4	6.0	800 kyr
Trizonia_fault	10.6	65	0	7	1.3	1.4	1.5	5.9	800 kyr
West_Channel_fault	10.8	45	0	2.5	0.4	0.45	0.5	5.6	240 - 400 kyr
South_Eratini_fault	12	45	0	6.5	0.6	1	1.4	6.0	800 kyr
East_Channel_fault	22	45	0	4.5	1	1.4	1.8	5.7	1500 kyr
North_Erratini_fault	11.5	60	0	6	2.4	4	5.6	5.9	12 kyr
Marathias_fault	17.4	60	0	6.5	1.39	1.4	1.41	6.1	400 kyr
1995_fault	14	35	8	12	0.5	3.2	7	6.0	5 yr
Pyrgos_fault	11	35	6	11	0.5	3.2	7	6.1	5 yr

Table 3 : Fault characteristics in Boiselet, 2014. Mmax calculated using Wells and Coppersmith equation for normal faults.

5

ANNEXE 1:

5